Pergamon

Solid State Communications, Vol. 101, No. 1, pp. 77–81, 1997

0038–1098/97 $17.00+.00

PII: S0038–1098(96)00377-8

MAGNETO-TRANSPORT SPECTROSCOPY ON A QUANTUM WIRE

A. Yacoby, H.L. Stormer, K.W. Baldwin, L.N. Pfeiffer and K.W. West

Bell Laboratories, Lucent Technologies, Murray Hill, NJ 07974, U.S.A.

(*Received* 13 *June* 1996; *accepted* 17 *June* 1996 *by A. Pinczuk*)

One-dimensional structures are expected to show unique electronic transport behavior as a consequence of the Coulomb interaction between carriers. A considerable number of theoretical predictions remain largely untested by experiment due to a lack of a suitable one-dimensional wire. Using a new crystal growth technique a unique tube-like structure with a cross section of 25 nm × 25 nm has been created in a semiconductor. The mean free path of the electrons exceeds 10 μm – more than 400 times the confinement dimension. The energy spacing between one-dimensional modes far exceed any random potential fluctuations and is more than 10 times larger than previously achieved by other techniques. The conductance plateaus of these wires deviate significantly from the expected universal values suggesting the relevance of electron–electron interactions. Copyright © 1996 Published by Elsevier Science Ltd

Keywords: A. nanostructures, B. epitaxy, C. electron–electron interactions, C. electronic transport.

Ever since it was realized that a one-dimensional (1D) electron system should show unique electronic properties [1, 2] have there been efforts to implement such a quantum wire, elucidate its energy spectrum and investigate its electronic transport. Beyond quantization of the conductance, eventually there is the expectation to observe deviations from traditional Fermi liquid behavior driven by the uniqueness of the electron–electron interaction in 1D [2–6]. A major challenge has been simply the fabrication of a suitable 1D structure [7, 8]. While quantum wires are expected to exhibit unique transport features, they are also exceptionally susceptible to potential fluctuations which easily localizes their carriers [9].

Of course, quantized conductance has been observed in quantum point contacts [1]. These are discrete, narrow constrictions in an otherwise two-dimensional flow. Being, in effect, zero-dimensional these structures are largely immune to inhomogeneities. However, they are not 1D. In fact, the existence of conduction quantization in a point contact severely complicates identification of 1D behavior. Observation of conductance plateaus in a wire cannot *per se* be taken as an indicator for one-dimensionality. Any accidentally narrow section along an otherwise arbitrary path can mimic the sought-after behavior. In this regard, the common method of preparing 1D systems by laterally squeezing a two-dimensional electron gas (2DEG) via metallic gates into a narrow stripe is particularly vulnerable. Their weak lateral confining potentials [1, 7, 8] hardly separates the subbands and they are easily mixed by the slightest inhomogeneity which destroys ballistic transport. And yet, conductance quantization may survive due to an accidental defect or narrow section along the stripe.

A "good" 1D wire with long ballistic mean free path must have the following attributes: First, potential fluctuations must be minimal to eliminate backscattering within each mode. Second, its carriers must be strongly confined in the lateral dimensions so as to widely separate the 1D subbands, prevent inter-mode scattering from residual inhomogeneities and avoid the accidental formation of a point contact. For true 1D transport to be present one needs to observe quantized plateaus in long, tube-like structure *and* demonstrate that their subband splitting largely exceed the strength of any anticipated potential fluctuation.

In this paper we introduce such quantum wires. They are fabricated by a new crystal growth technique which tightly confines the electrons on three sides by atomically smooth semiconductor hetero-junctions. Confinement

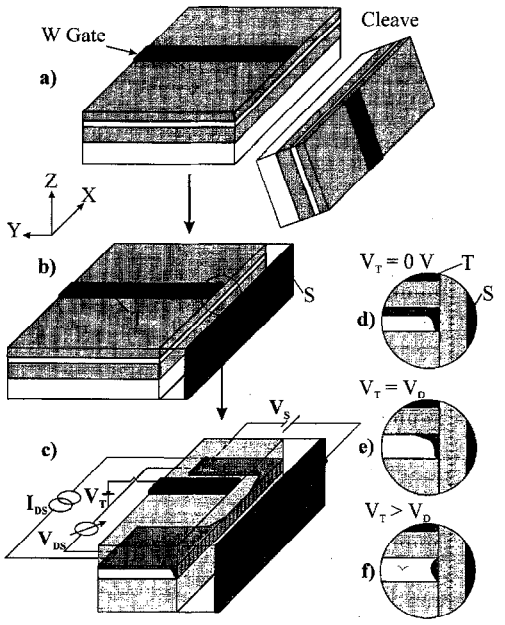

Fig. 1. (a) Sample geometry: A sketch of the first MBE growth consisting of a modulation doped quantum well (narrow white layer) clad by two layers of AlGaAs (gray layers). The long and narrow tungsten stripe (T) is deposited onto the structure. After cleaving the sample the T-gate ends at the cleavage plane. (b) The second modulation-doped MBE growth (δ-doped AlGaAs) along the 1 1 0 direction (transparent layer). A standard Ti–Au gate (S) is deposited over the entire 1 1 0 surface. (c) A blow up of the critical device region along with the electronic circuitry. The hatched region denotes the electron system. The top gate (T) is biased to deplete the 2DEG underneath, leaving only the wire as a possible conduction channel. (d) A cross section through the y–z-plane in the wire region for the unbiased conditions. The 2DEG is coupled directly to the electrons along the cleaved edge. In the ungated region this is the path by which current from the 2DEG enters and leaves the wire. (e) The 2DEG is depleted by the top gate. This is the least negative top gate voltage for which the quantum wire is defined. (f) For larger (negative) values of the top gate the wire confinement improves and its density is reduced.

in the fourth dimension is provided by a strong electric field. The transport mean free path of the 1D electrons is as long as 10 μm. Magneto-transport measurements reveal the symmetries and the energies of the wavefunctions of the quantum wire. The subband separation is determined to be in excess of 20 meV, well above any common potential fluctuations in this high-quality MBE material.

Wire fabrication by cleaved edge overgrowth (CEO) [10] and the unique, *in situ* contacting scheme are shown in Fig. 1. The starting point is a modulation-doped GaAs quantum well of 14 nm, 25 nm or 40 nm thickness embedded between two thick AlGaAs layers and doped from the top (Fig. 1a). The resulting 2DEG resides 500 nm below the top surface, has an electron density $n \sim 1\text{–}2 \times 10^{11}\,\mathrm{cm}^{-2}$ and a mobility $\mu \gtrsim 3\times 10^{6}\,\mathrm{cm}^{2}\,\mathrm{Vs}^{-1}$. A long and narrow evaporated tungsten stripe (Fig. 1a) has two purposes. First, it acts as a top (T) gate to separate the 2DEG into two halves defining the right and left contact to the 1D wire. Second, its width (from 1 μm to 20 μm) establishes the length of the quantum wire. The quantum wire itself is fabricated by cleaving the specimen in ultra-high vacuum and overgrowing the smooth cleavage plane with a second modulation-doping sequence (Fig. 1a, b). This introduces electrons at the edge of the quantum well (see Fig. 1d). The quality of the growth on the cleaved surface is monitored by growing simultaneously on a (1 1 0) reference wafer. The 2DEG formed on the reference wafer has a density of typically $3 \times 10^{11}\,\mathrm{cm}^{-2}$ and a mobility of $1.3 \times 10^{6}\,\mathrm{cm}^{2}\,\mathrm{Vs}^{-1}$. From this we infer a similarly high quality growth on the cleaved plane. The cleave also defines the end of the tungsten gate. Figure 1c shows a blow-up of the critical device region under suitable bias conditions. Ohmic contacts to the 2D system are made far away from this region by diffusing Indium-dots into the 2DEG. In essence, the top gate (T) primarily serves to separate the 2D sheets that contact the 1D wire whereas the side gate (S) only 200 nm from the wire primarily serves to vary the electron density in the 1D system.

Figures 1d, e, f show a schematic cross sections of charge distributions in the wire region for different top gate voltages V_T. For $V_T = 0$ the 2DEG is continuous and the 2D contact areas are not yet separated. For a negative voltage $V_T = V_D$ (2DEG depletion voltage) the top gate has separated the contact area but the connecting wire (here seen in cross section) remains weakly confined (Fig. 1e). For V_T yet more negative the 1D wire is well developed and firmly confined in two dimensions: in the z-direction by the quantum well and in the y-direction by the strong triangular potential of the cleaved-edge modulation-doping sequence. It is important to realize that both gates affect the electron density in the wire as well as the shape of the confining potential. However, to first order, the potential in the z-direction is always dominated by the strong well potential and, for our operating conditions, is minimally altered by either V_S or V_T. The triangular potential in the y-direction, on the other hand, is considerably modified by both gates, although to somewhat different extent. For strongest 1D confinement we bias the top gate negative and the side gate strongly positive pushing the electrons against the cleaved edge of the quantum well.

Electronic transport measurements on the quantum wire are performed at 300 mK, using an excitation of $V_{ex} = 10\,\mu$V, 16 Hz in the contact configuration of

Fig. 1c and measuring the source-drain voltage V_{SD} and current I_{SD}. Figure 2 shows the differential conductance, $g = \mathrm{d}I_{SD}/\mathrm{d}V_{SD}$, of a 1.5 μm long quantum wire in a 40 nm quantum well as a function of top gate voltage V_T and for several different side gate voltages V_S. Clear conductance steps are observed which move to less negative values of V_T as V_S is reduced. They are a direct consequence of the decrease in the 1D electron density caused by V_T depleting successive 1D subbands.

Our first goal is to establish the high quality of the quantum wire fabricated by this CEO-technique. The inset of Fig. 2 shows the last plateau for wires of five different lengths fabricated consecutively along the edge of a single CEO specimen. The plateaus are flat up to a length of 10 μm and their conductance value remains practically constant from 1 μm to 5 μm. The flatness of a plateau indicates the lack of backscattering and, hence, is a good indication of the quality of a wire. From the persistence of the plateaus in the inset to Fig. 2, we deduce a mean free path of more than 10 μm in CEO devices. While we infer ballistic transport over such long distances, we realize that the conductance plateaus are not multiples of $2e^2/h$. The lowest mode, corresponding to the last plateau in Fig. 2, has a conductance value of $g = 1.8e^2/h$ and the second mode contributes only an additional $0.9e^2/h$. The third and fourth modes again contribute conductances just slightly below $2e^2/h$.

Such non-universal values of the plateaus are observed in all of our samples. The last plateau deviates from the universal conductance value by as much as 25% in the 25 nm and 14 nm quantum well devices (see inset to Fig. 2). However, the conductance values are *exactly reproduced in all devices* fabricated from the same quantum well material, even when cleaved and overgrown during different runs. The deviations of the plateau values from $2e^2/h$ is *therefore not an artifact* of a particular quantum wire and its unique potential variations. Furthermore, the plateaus approach their universal values as the temperature rises, seemingly saturating at the correct multiples of $2e^2/h$. At present we do not understand the origin of this behavior. We speculate that either e–e interaction within the quantum wire [5] or an intricate coupling between the 2DEG reservoirs and the wire are the source for this unique

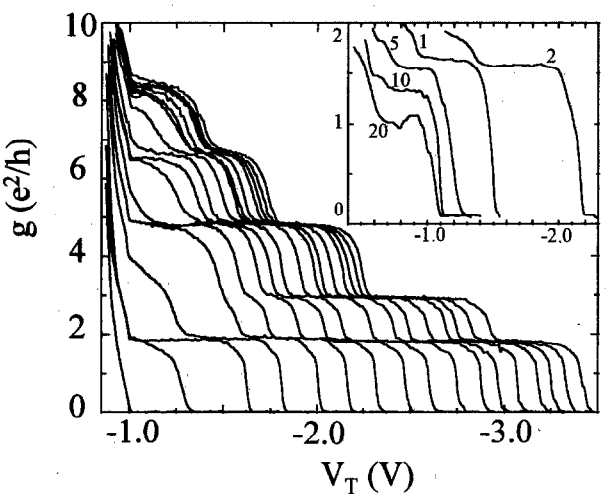

Fig. 2. Differential conductance $g = \mathrm{d}I_{DS}/\mathrm{d}V_{DS}$ of 1.5 μm long wire in a 40 nm quantum well vs the top gate voltage (V_T) taken at 50 meV steps between $V_S = -0.2$ V (left most curve) and $V_S = +0.6$ V (right most curve). The wire is first formed at $V_T = V_D \approx -1$ V. Inset: differential conductance of the last plateau for wires of different lengths fabricated consecutively along the edge of a single 25 nm CEO specimen. The numbers denote the wire length in microns.

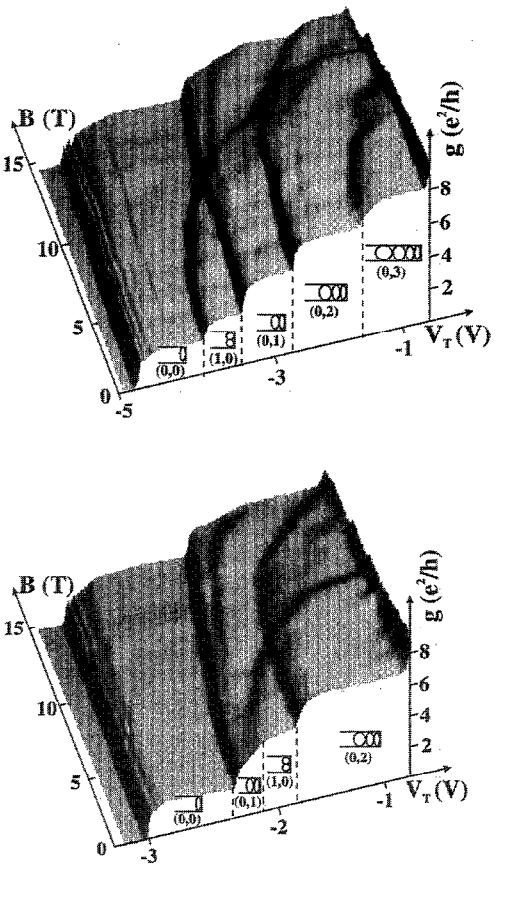

Fig. 3. 3D plots of a small differential conductance of a 2 μm long wire in a 25 nm quantum well as a function of V_T and a magnetic field along the y-direction for two different side gate voltages: (a) $V_S = +1.0$ V, (b) $V_S = +0.62$ V. At the vertical steps the Fermi energy coincides with the bottom of the respective 1D subband. The sketches show the electron density profile of the highest populated mode in the wire, in a geometry similar to Fig. 1f. Two quantum numbers (i, j) identify the wavefunction in the z and y directions, respectively.

observation. In the remainder of the text we focus on studying the confinement potential and energy levels of our CEO wires.

Figure 2 already provides some hint as to the energetic structure of the quantum wire. The second plateau contributing $0.9e^2/h$ vanishes for small values of the parameter V_S, whereas the first and third plateaus remain well defined. This suggests that for such values of the side gate voltage V_S, the second and third wire mode are energetically almost degenerate and consequently the conductance value jumps by two units directly from the first to the third plateau.

In order to reach a better understanding of the confinement potential and energy level sequences, we conducted systematic measurements of the wire conductance in magnetic fields up to 14.5 T [11]. Figure 3a shows a 3D plot of the differential conductance of a 2 μm long wire fabricated from a 25 nm quantum well as a function of the top-gate voltage V_T and the magnetic field in the y-direction. Since the steps correspond to 1D modes crossing the Fermi energy, their motion reflects the magnetic field dependence of the mode energies. With increasing magnetic field all subbands move to less negative values of V_T suggesting that the energies of the associated 1D modes are approaching E_F. As in Fig. 2, the second level again stands out by moving much more rapidly than the rest.

In order to understand the data of Fig. 3a we make a simplifying assumptions about the confining wire potential: in the z-direction it consists of a square well and in the y-direction it is triangular and tunable through V_S. Since such a simplified potential is separable, we can assign two quantum numbers (i, j) to each mode; i identifying the state in the z-direction, j in the y-direction. A B-field in the y-direction preferentially affects "rectangular (i) modes", whereas a field in the z-direction preferentially affects the "triangular (j) modes". The inset to Fig. 3a shows sketches of some examples. Inspecting these wavefunctions one realizes that for $B \| y$ the high-field asymptotic energy is $E_j + (i + 1/2)\hbar\omega_c$ whereas for $B \| z$ this limit is $E_i + (j + 1/2)\hbar\omega_c$. Here $\hbar\omega_c$ represents the cyclotron energy and E_i and E_j are the energies of the i and j modes, respectively, in the absence of a B-field. Since levels 1, 3 and 4 have a weak field dependence in Fig. 3a whereas level 2 crosses levels 3 and 4, we assign the sequence (0, 0), (1, 0), (0, 1), and (0, 2) to these lowest four quantum wire modes. The exceptional nature of the second level, displaying an extra node in the z-direction, is probably related to its particularly low conductance value in Fig. 2. This would favor a wavefunction-dependent coupling between the 2DEG states and the quantum wire states as the source for the non-universal values of the conductance plateaus. Level 5 is somewhat ambiguous. Based on an approximate calculation of the E_is and E_js we favor the assignment (0, 3) although it being the (1, 1) mode cannot be excluded. We can further support the assignment for the four lowest states by taking data such as in Fig. 3a for different side gate voltages V_S. The expectation is, that with less positive V_S, the triangular potential becomes softer, decreasing the energy separation of the j-states in (i, j). The side gate voltage V_S should then allow us to shift the rectangular mode (1, 0), which is largely unaffected by V_S, through the triangular modes (0, j). This is exactly the behavior observed in Fig. 3b which shows the case for a smaller V_S in the same 25 nm specimen. We further substantiate our assignment by performing these measurements on the 40 nm and 14 nm CEO specimens. Data from both thicknesses are consistent with the above interpretation. For the 40 nm sample we observe a smaller rectangular vs triangular confinement. In the 14 nm sample, on the other hand, the (1, 0) mode is not seen at all which indicates a larger rectangular vs triangular confinement as compared to the 25 nm case.

Figure 3 not only determines the symmetry and sequence of the wire modes, but also provides a value for their energetic splitting. We use again our simplified model of separable potentials. In this model, the lowest two modes of Fig. 3a differ only in their z-confinement which is predominantly due to the rectangular potential of the square well. For a 25 nm well the calculated splitting of the lowest two eigenstates is $\approx$20 meV and, hence, the splitting between the lowest two eigenmodes [(0, 0) and (1, 0)] of the quantum wire in Fig. 3a is $\approx$20 meV. The splitting between the lowest and the third mode of Fig. 3a, corresponding to the ground state and first excited state of the triangular well, is necessarily larger than 20 meV. This asserts that the strength of confinement of the electrons in the y-direction, at least for the lowest two modes, is comparable to or even stronger than the confinement in the z-direction. From this we conclude that the 1D modes of the 25 nm CEO structure are confined to an area of about 25 nm $\times$ 25 nm. Our wires, therefore, have a tube-like shape with an aspect ratio as high as 1 : 1 : 400 and a subband separation in excess of 20 meV. This is in contrast to the traditional narrow stripe geometry which generates substantially weaker confinement ($\approx$1 meV). The 14 nm quantum well (not shown) is yet more strongly confined and shows splittings beyond 20 meV. All in all our magneto transport spectroscopy confirms the exceptionally high quality of CEO fabricated 1D wires and their extremely robust 1D transport behavior.

For completeness we have also measured the wire conductance when the magnetic field is applied in the x-direction and in the z-direction. In the first case, as expected, the levels are just slightly affected by the

magnetic field, indicating again a wire cross section comparable to the typical 13 nm cyclotron diameter at 14.5 T. The data for $B \| z$ further support our assignment of the wire states but are considerably more complex than Fig. 3 since the wire conductance is now superimposed onto the Shubnikov–de Haas oscillation of the 2DEG in the contacting areas. Due to their complexity, we can only provide a qualitative description.

The most striking observation is that the steps from the 1D subband quantization (similar to Fig. 3) seem to terminate at specific B-field values corresponding to specific, integer Landau level filling factors ν of the 2DEG. For example, under the same V_S as in Fig. 3a the third level $(0,1)$ terminates at $\nu = 2$ (both spin orientations of lowest Landau level occupied). The fourth level $(0,2)$ terminates at $\nu = 4$ and the fifth level $(0,3)$ terminates at $\nu = 6$. This behavior suggests that for $B \| z$ the 2DEG couples into 1D wire modes through its quantized edge states and that this coupling is adiabatic. Once the filling factor in the 2DEG drops below a given Landau level and its associated edge mode, the corresponding wire mode is no longer fed. Such adiabatic coupling between the chiral 1D edge modes of the 2DEG in a B-field and the regular 1D modes of the quantum wire is an intriguing aspect of this geometry.

In conclusion, we have demonstrated high quality 1D quantum wires based on cleaved edge overgrowth in molecular beam epitaxy. Electrons are confined to less than 25 nm in both confinement directions leading to subband separation in excess of 20 meV. Their transport mean free path exceeds 10 μm. Through magneto-transport experiments we are able to extract spectroscopic information on the energy level scheme as well as on the symmetry of the eigenstates in the two confining directions. Beyond our wire spectroscopy, these high-quality, robust quantum wires provide a sound basis for the investigation of pure 1D systems. The non-universal values of the conductance plateaus and their temperature dependence may already hint at the relevance of electron–electron interactions in such wires.

Acknowledgements—We would like to thank N.S. Wingreen for fruitful interactions. We are also indebted to H.U. Baranger, J.P. Eisenstein, S. He, Y.B. Kim, A. Schmeller and R.K. Smith for extensive discussions.

REFERENCES

1. Beenakker, C.W.J. and von Houten, H., in *Solid State Physics, Semiconductor Heterostructures and Nanostructures* (Edited by H. Ehrenreich and D. Turnbull). Academic Press, New York, 1991.
2. E.g. *Highly Conducting One Dimensional Solids* (Edited by J.T. Devreese). Plenum Press, New York, 1979.
3. Haldane, F.D.M., *J. Phys.*, **C14,** 1981, 2585.
4. Apel, W. and Rice, T.M., *Phys. Rev.*, **B26,** 1992, 7063.
5. Kane, C.L. and Fisher, M.P.A., *Phys. Rev.*, **B46,** 1992, 15233.
6. Tarucha, S., Honda, T. and Saku, T., *Solid State Commun.*, **94,** 1995, 413.
7. E.g. *Nanostructure Physics and Fabrication* (Edited by M.A. Reed and W.P. Kirk). Academic Press, New York, 1989.
8. Honda, T., Tarucha, S., Saku, T. and Tokua, Y., *Jpn. J. Appl. Phys.*, **34,** 1995, L72.
9. Abrahams, E., Anderson, P.W., Licciardello, D.C. and Ramakrishnan, T.V., *Phys. Rev. Lett.*, **42,** 1979, 673.
10. Pfeiffer, L.N., Stormer, H.L., Baldwin, K.W., West, K.W., Goni, A.R., Pinczuk, A., Ashoori, R.C., Dignam, M.M. and Wegscheider, W., *J. Crystal Growth*, **849,** 1993, 127.
11. Wang, J., Beton, P.H., Mori, N., Eaves, L., Buhmann, H., Mansouri, L., Main, P.C., Foster, T.J. and Heinini, M., *Phys. Rev. Lett.*, **73,** 1994, 1146.